2

Structure, Morphology, and Optical Properties of the Compact, Vertically-Aligned ZnO Nanorod Thin Films by the Solution-Growth Technique

Chu-Chi Ting
Graduate Institute of Opto-Mechatronics Engineering, National Chung Cheng University, Chia-Yi, Taiwan, R.O.C.

1. Introduction

ZnO is a direct band gap semiconductor with hexagonal wurzite crystal structure (a = 0.325 nm, c = 0.520 nm), and has a wide band gap of 3.37 eV at 300 K (Kligshirn, 1975), large exciton binding energy of 60 meV (Özgür et al., 2005), and high refractive index ($n_{550\ nm}$ = 2.01). ZnO thin films have attracted many researchers to study because of its good optical and electrical characterizations for the applications to light-emitting diodes (Saito et al., 2002), field emitters (Zhu et al., 2003), and solar cells (Lee et al., 2000).

There are many methods for the fabrications of ZnO films such as metal-organic chemical vapor deposition (Yang et al., 2004), laser ablation (Henley et al., 2004), and sputtering (Jeong et al., 2003). However, most of technologies are correlated to the vacuum and high-temperature processes, which results in the high cost. In recent years, the solution-growth route has been used to fabricate the ZnO nanorod thin films (Vayssieres, 2001, 2003; Li et al., 2005; Tak & Yong, 2005; Lee et al., 2007). Vayssieres *et al*. developed the large three-dimensional (3D) and highly oriented porous microrod or nanorod array of n-type ZnO semiconductor by the equimolar (0.1 M) aqueous solution of zinc nitrate [$Zn(NO_3)_2$ $6H_2O$] and methenamine ($C_6H_{12}N_4$) at low temperature. The crystallographic faces of well-aligned single-crystalline hexagonal rods are perpendicularly grown along the [001] direction onto the substrate, resulting in the formation of very large uniform rod arrays (Vayssieres, 2001, 2003). Tak and Yong demonstrated that uniform ZnO nanorods were grown on the zinc-coated silicon substrate by the aqueous solution method containing zinc nitrate and ammonia water. Although the growth mechanism of ZnO nanorods in an organic amine solution has not completely been understood, there are several parameters influencing the growth characteristics (i.e., width, length, growth rate, and preferred orientation) of ZnO nanorods such as growth temperature, growth time, zinc ion concentration, pH of solution, and ZnO seed-layer morphology, which can be applied to control the tailored growth dimensions and orientation of ZnO nanorods (Li et al., 2005; Lee et al., 2007; Tak & Yong, 2005; Vayssieres, 2001, 2003).

It is noted that the surface morphology of ZnO nanorod thin films developed by Vayssieres *et al*. exhibited hexagonal-shaped nanorods and many unfilled inter-columnar voids

between nanorods (Vayssieres et al., 2001). However, this kind of hexagonal surface morphology is obviously different from that of other oxide films (*e.g.*, TiO_2, SiO_2, SnO_2, and ZrO_2) fabricated by other solution-growth routes such as chemical bath deposition (CBD) and liquid phase deposition (LPD) (Kishimoto et al., 1998; Lin et al., 2006; Mugdur et al., 2007; Tsukuma et al., 1997). In general, the films synthesized by CBD or LPD exhibits the spheroidal grain morphology. We found that hexagonal-shaped ZnO nanorod thin films with less voids can be synthesized under specific processing parameters and their optical properties are similar to that of ZnO films prepared by sputtering methods. Although there are extensive reports on the structural and physical properties of ZnO nanorod thin films prepared by solution methods, few reports are available on the preparations and characteristic investigations of high packing-density ZnO nanorod thin films.

In this chapter, we fabricated the dense and well-aligned ZnO nanorod thin films by the simple solution method. Structural and optical properties of the resulting ZnO nanorod thin films were systematically examined in terms of the structural evolution of the films at different zinc ion concentrations, growth temperatures, growth time, growth routes, and ZnO seed-layer morphology. We believe that the dense and well-aligned ZnO nanorod thin films fabricated by solution-growth method can satisfy the basic requirement of optical-grade thin films, and has the merits of low temperature, large scale, and low cost.

2. Fabrication of the solution-growth ZnO nanorod thin films

2.1 Fabrication of ZnO seed layers

The ZnO-coated glass substrate acted as the seed layer for the growth of well-aligned ZnO nanorods in aqueous solution. The ZnO seed-layer thin films were fabricated by sol-gel spin-coating technology. 2-methoxyethanol (2-MOE, $HOC_2H_4OCH_3$, 99.5%, Merck) and monoethanolamine (MEA, $HOC_2H_4NH_2$, ≥ 99%, Merck) with molar ratio of Zn/2-MOE/MEA= 1/21/1 were first added to zinc acetate [$Zn(CH_3COO)_2$, 99.5%, Merck], followed by stirring for 10 h to achieve the sol-gel ZnO precursor solution. Then the ZnO precursor solution was spin-coated on silica glass substrates (Corning, Eagle 2000). The as-deposited sol-gel films were first dried at 100 °C/10 min, pyrolyzed at 400 °C/10 min, and further annealed at 400-800 °C/1 h to achieve the seed-layer ZnO thin films with an average grain sizes of 20-100 nm and a thickness of ~90 nm.

2.2 Fabrication of ZnO nanorod thin films

For the fabrication of solution-grown ZnO nanorod thin films, the ZnO seed-layer substrates were deposited in the Zn^{2+} aqueous solutions which were compose of the mixture of zinc nitrate [$Zn(NO_3)_2$ $6H_2O$, ≥ 99%, Merck], hexamethylenetetramine (HMT, $C_6H_{12}N_4$, ≥ 99 %, Merck), and H_2O with molar ratio of Zn/HMT/H_2O=0.1-1/1/1000 to make 0.005-0.05 M zinc ion solutions. The growth temperatures and time were precisely controlled at 55-95 °C and 1.5-6 h, respectively. The multiple-stepwise and one-step solution-growth routes were employed to the growth of the ZnO nanorod thin films. Figure 1 depicts the schematic flowchart of the multiple-stepwise and one-step solution-growth routes for the fabrication of ZnO nanorod thin films. For example, for the ZnO nanorod thin film grown at 75 °C/6 h by the multiple-stepwise route, the ZnO seed-layer substrate was first immersed in the growth solution, and then the growth solution was heated at 75 °C for 1.5 h. After ZnO nanorods

growth, the ZnO nanorod thin film was removed from the solution and we immediately put it in another new growth solution, and then the growth solution was heated at 75 °C for another 1.5 h. The same process was repeated 2-4 times and the total growth time was accumulated from 3 to 6 h. On the other hand, the substrate was immersed in the growth solution at 75 °C for continuous 6 h for the one-step route.

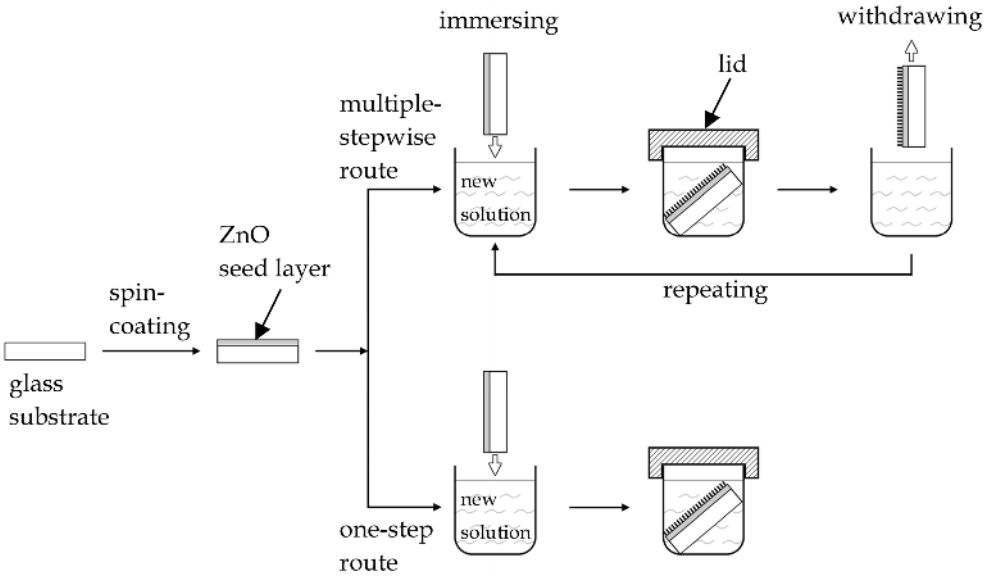

Fig. 1. Schematic flowchart of the multiple-stepwise and one-step solution-growth routes for the fabrication of ZnO nanorod thin films.

2.3 Measurement of physical properties

The crystal structure was detected by an X-ray diffractometer (Shimadzu, XRD 6000). Scanning electron microscope (Hitachi, S4800-I) was used for microstructural examination. The thickness of ZnO films was measured by the α-step profile meter (KLA-Tencor, Alpha-Step IQ). Transmission spectra in the UV and visible ranges were determined on a Shimadzu UV-2100 spectrophotometer. Samples were excited by using a 325 nm He-Cd laser with an output power of 4 mW at room temperature. the UV and visible fluorescence was detected by spectrophotometer (Horiba Jobin-yvon, iHR 550) equipped with a photomultiplier tube detector (Hamamatsu, 7732P-01) at room temperature.

3. Structure, morphology, and optical properties of the compact, vertically-aligned ZnO nanorod thin films

3.1 Film morphology

In our experiments, the zinc ion concentrations were adjusted from 0.005 to 0.05 M, the growth temperatures were controlled from 55 to 95 °C, the growth time was selected in the range of 1.5 to 6 h, the grain sizes of ZnO seed layer varied from 20 to 100 nm, and two kind

of growth routes, i.e., multiple-stepwise and one-step route, were used. However, the most compact and densest ZnO nanorod thin film with the thickness of ~800 nm can only be fabricated under very specific conditions, i.e., 0.05 M, 75 °C, 6 h, multiple-stepwise route, and ZnO seed layer with an average grain size of ~20 nm. Figs. 2(a)-(j) illustrate the top-view and cross-sectional scanning electron microscopy (SEM) imagines of ZnO nanorod thin

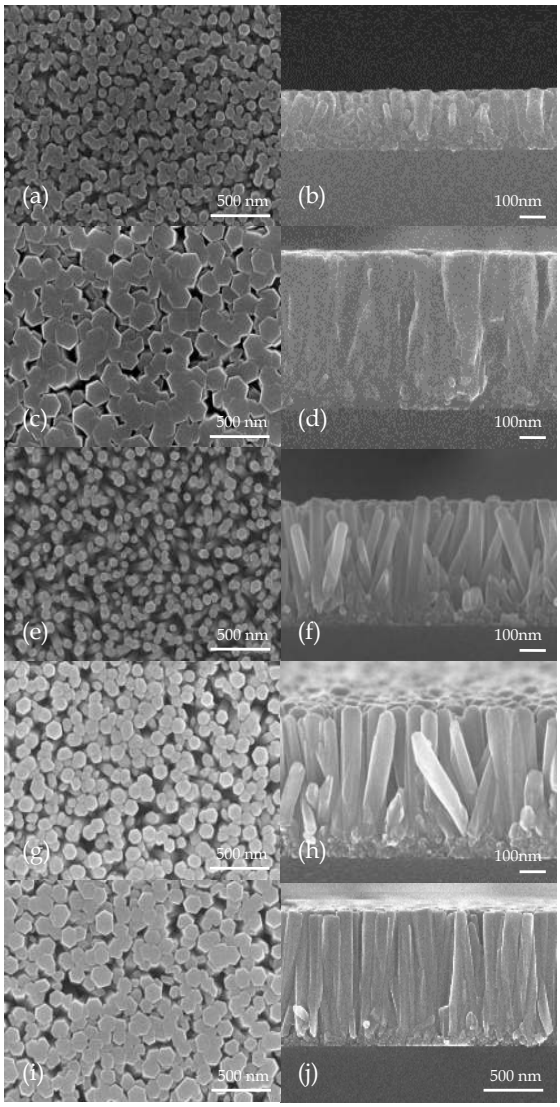

Fig. 2. Top-view and cross-sectional SEM imagines of ZnO nanorod thin films fabricated under the conditions of 0.05 M, seed-layer grain size of ~20 nm, and (a, b) 75 °C/1.5 h (multiple-stepwise route), (c, d) 75 °C/6 h (multiple-stepwise route), (e, f) 95 °C/1.5 h (multiple-stepwise route), (g, h) 75 °C/4.5 h (one-step route), and (i, j) 75 °C/6 h (one-step route).

films fabricated under the conditions of 0.05 M zinc ion concentration, ZnO seed layer with an average grain size of ~20 nm, different growth temperatures/time, and different solution-growth routes (one-step and multiple-stepwise routes). Obviously, the surface morphology of ZnO nanorod thin film fabricated by multiple-stepwise route at 75 °C/6 h exhibits larger aggregated hexagonal grains and more compact structure than others', as shown in Figs. 2(c) and 2(d). Cross-sectional SEM image also exhibits well-developed and larger fused columnar grains, which is very similar to the sputtered thin films (Mirica et al., 2004). However, for the ZnO nanorod thin film fabricated at 95 °C/1.5 h, the film is obviously composed of a large bundle of the ZnO nanorods and most of nanorods do not fuse together, as shown in Figs. 2(e) and 2(f), which resulted in the formation of lots of unfilled inter-columnar volume between nanorods. In addition, some ZnO nanorods do not vertically align very well and they are inclined to the substrate surface.

Figure 3 shows the average diameters and lengths versus growth time and temperatures of ZnO nanorods prepared under the conditions of 0.05 M, one-step route, multiple-stepwise route, and ZnO seed layer with an average grain size of ~20 nm. The diameter and length of ZnO nanorod thin films fabricated by multiple-stepwise route at 95 °C/6 h are ~240 and ~2300 nm, respectively, which is obviously larger than that of ZnO nanorod thin films fabricated by multiple-stepwise or one-step route at 75 °C/6 h. Therefore, the higher growth temperature can induce ZnO nanorods with larger diameter and length, consistent with others' investigations (Li et al., 2005; Lee et al., 2007; Tak & Yong, 2005; Vayssieres, 2001, 2003).

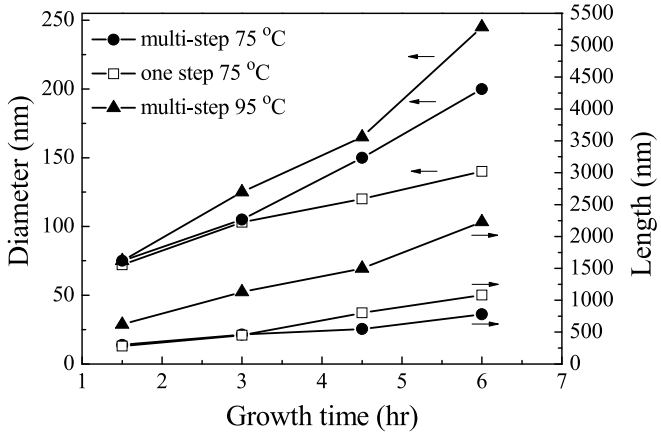

Fig. 3. Average diameters and lengths of ZnO nanorod thin films fabricated under the conditions of 0.05 M, seed-layer grain size of ~20 nm, different growth methods (one-step route and multiple-stepwise route), growth temperatures, and growth time.

For the ZnO nanorod thin films fabricated at 75 °C/1.5 h, short nanorods with the diameters of 60-80 nm and the height of ~200 nm are very crowded and combined each other at side faces, as shown in Figs. 2(a) and 2(b). Further increase in growth time to 6 h causes the highly c-axis-oriented hexagonal ZnO grains (as shown in Figure 4 in the next section) to coalesce and form larger aggregated hexagonal grains with the average diameter of ~200 nm and the height of ~800 nm, resulting in the reduction of unfilled inter-columnar volume and voids [see Figs. 2(c) and 2(d)].

Compared the SEM images of ZnO nanorod thin films fabricated by multiple-stepwise route at 75 °C/6 h [Figs. 2(c) and 2(d)] with that fabricated by one-step route at 75 °C/6 h [Figs. 2(i) and 2(j)], the former exhibited the larger aggregated hexagonal grains and fused columnar structure with the average diameter of ~200 nm and the height of ~800 nm; however, the latter exhibited the smaller aggregated hexagonal grains with the average diameter of ~140 nm and the height of ~1100 nm.

3.2 Crystal structure

Figure 4 shows the X-ray diffraction (XRD) patterns of ZnO nanorod thin films fabricated under growth temperatures, growth time, multiple-stepwise route, and the ZnO seed layer with an average grain size of ~20 nm. Obviously, all of the XRD patterns exhibits only one diffraction peak and the peak position at ~34.53-34.57°, i.e. (002) is the characteristic of wurzite ZnO (JCPDS No. 36-1451). Hence, these ZnO nanorod thin films possess highly preferred orientation with c-axis normal to the substrate.

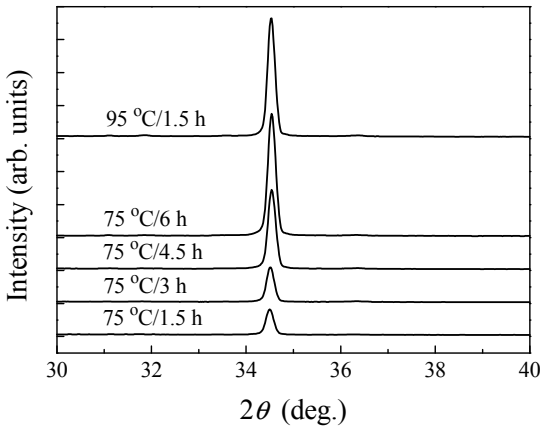

Fig. 4. XRD patterns of ZnO nanorod thin films fabricated under the conditions of 0.05 M, seed-layer grain size of ~20 nm, multiple-stepwise route, and different growth temperatures/time.

The diffraction intensity of ZnO nanorod thin film prepared at 75 °C /6 h is similar to that of ZnO nanorod thin film prepared at 95 °C/1.5 h, which implies that they have similar crystallinity because of similar thickness (~ 800 nm) between these two samples. Although the 75 °C growth temperature is much lower than 95 °C, these coalesced and aggregated hexagonal nanorods fabricated at 75 °C still possess good crystallinity in comparison with the uncoalesced and well-shaped hexagonal nanorods fabricated at 90 °C and possessing the single crystalline nature (Li et al., 2005). However, the photoluminescence (PL) spectra show that ZnO nanorod thin film prepared at 75 °C/6 h had more oxygen defects as compared with that prepared at 95 °C/1.5 h, and this phenomenon will be discussed in the section of optical properties.

In addition, the (002) peak position of ZnO nanorod thin films prepared at 75 °C/1.5-6 h deviates from the randomly orientated ZnO powder value (34.42°) and shifts toward higher

value, indicating the compressive stress existing in these extremely c-axis-oriented ZnO nanorod thin films (Sagar et al., 2007). The (002) peak position progressively varies from 34.50° to 34.54° by increasing growth time, which means that the compressive stress increases with the increase of thickness and aggregated hexagonal grain size. After calculation, the strains vary from -0.21 to -0.32% (Puchert et al., 1996).

3.3 Grown mechanisms of compact, vertically-aligned ZnO nanorod thin films

Some growth characteristics such as average diameters and lengths of ZnO nanorods could be determined by some significant parameters such as the morphology of a zinc metal seed layer, pH, growth temperature, and concentration of zinc salt in aqueous solution (Tak & Yong, 2005). Li *et al*. proposed the growth mechanism of ZnO nanorods fabricated by the aqueous solution method. The proposed mechanism includes three steps: (1) fine and independent ZnO nanorods grew and bundled together. (2) fine ZnO nanorods coalesced. (3) single large dimension hexagonal ZnO nanorod was formed (Li et al., 2005). Lee *et al*. systematically examined that the degree of alignment of dense ZnO nanorod arrays synthesized via a two-step seeding and solution-growth process was significantly influenced by the ZnO seed layer roughness. The highly c-axis aligned and dense ZnO nanorods can be obtained during the roughness of ZnO seed layer was ≦ 2 nm (Lee et al., 2007).

Vayssieres pointed that the diameter of ZnO nanorods could increase 10 times from 100-200 nm to 1000-2000 nm when the zinc ion concentration increased from 0.001 M to 0.01 M (Vayssieres, 2003). The higher zinc ion concentration can accelerate a smaller bundle of ZnO nanorods to coalesce together and form larger dimension ZnO nanorods for reducing the surface energy (Li et al., 2005). Hence, the zinc ion concentration can obviously influence the diameter of ZnO nanorods. For the one-step route, the growth solution is limited in a closed system. When the growth time increases, the zinc ions will be gradually depleted and the zinc ion concentration on the top of nanorods should be less than the initial solution, which reduces the lateral aggregation rate of hexagonal nanorods, induces the continuous growth of nanorods in vertical direction, and results in the nanorods with smaller diameter and larger length. However, multiple-stepwise route can supply and maintain the zinc ion concentration and accelerate the lateral coarsening growth of nanorods, which leads to the aggregation of hexagonal nanorods and the formation of close-packed columnar structure with larger diameter and shorter length. The growth mechanism of ZnO nanorod thin film prepared at 75 °C/1.5-6 h (multiple-stepwise route) is depicted in Figure 5. In addition, the formation of ZnO nanorods can be attributed to the following reaction equations (Li et al., 2005).

$$(CH_2)_6N_4 + 6H_2O \rightarrow 6HCHO + 4NH_3 \quad (1)$$

$$NH_3 + H_2O \rightleftarrows NH_4^+ + OH^- \quad (2)$$

$$2OH^- + Zn^{2+} \rightarrow ZnO_{(s)} + H_2O \quad (3)$$

On the other hand, the (002) plane in ZnO structure has the highest atomic density and possesses the lowest surface free energy. Therefore, the growth of a preferred *c*-axis oriented ZnO nanorod thin films can be easily driven at such low growth temperature. Additionally,

Lee *et al*. pointed that the surface morphology of ZnO seed layer can also significantly influence the prefer-oriented growth of ZnO nanorods (Lee et al., 2007). The smaller surface roughness of ZnO seed layer can induce the growth of ZnO nanorod with highly c-axis preferred orientation. In our system, when the grain size of ZnO seed layer is larger than 20 nm, the (100) and (101) diffraction peaks can be detected (XRD patterns are not shown here), which indicates that some ZnO nanorods do not vertically align very well and are inclined to the substrate surface. The ZnO seed layer with larger grains has higher roughness and can induce the formation of inclined ZnO nanorods and more unfilled inter-columnar voids between ZnO nanorods, as described in some published literatures. (Lee et al., 2007; Zhao et al., 2006) This phenomenon results in the ZnO nanorod thin films with lower densification and transmittance. The influence of ZnO seed-layer morphology on the preferred orientation of resulting ZnO nanorod thin films will be the subject of a separate study in the future.

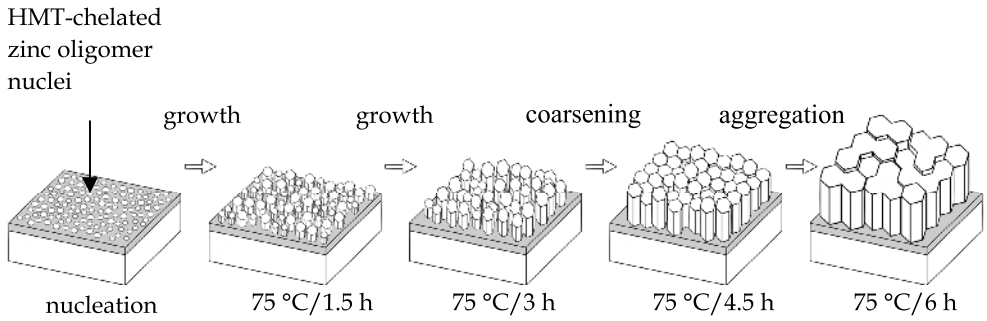

Fig. 5. Growth mechanism of ZnO nanorod thin film prepared at 75 °C/1.5-6 h (multiple-stepwise route).

3.4 Optical properties

3.4.1 Optical transmittance spectra

Figures 6(a)-6(c) show the optical transmittance spectra of ZnO nanorod thin films fabricated at 75 °C/1.5-6 h (multiple-stepwise route), 75 °C/1.5-6 h (one-step route), and 95 °C/1.5-6 h (multiple-stepwise route), respectively. The obvious interference fluctuation in the transmission spectra of ZnO nanorod thin films fabricated at 75 °C/1.5-6 h (multiple-stepwise route) are due to the interference phenomena of multiple reflected beams between the three interfaces: air-ZnO nanorods film, ZnO nanorods film-silica glass, and silica glass-air. The average visible transmittance calculated in the wavelength ranging 400-800 nm of the ZnO nanorod thin films fabricated at 75 °C for 1.5, 3, 4.5, and 6 h are 87.9, 87.5, 84.9, and 84.7%, respectively. Generally, there are three factors influencing the transmittance of ZnO nanorod thin films: (a) surface roughness, (b) defect centers, and (c) oxygen vacancies (Mohamed et al., 2006). In our system, the decrease of transmittance for the ZnO nanorod thin films fabricated at 75 °C for 1.5, 3, 4.5, and 6 h with the 100-800 nm in thickness could be related to two factors. One is the thicker ZnO nanorod thin films had larger hexagonal grain size and larger surface roughness. The other is the higher absorption effect for thicker films. The absorption coefficient can increase with the present of oxygen vacancies which is disclosed by the PL spectra (Figure 9) in the next section. Moreover, it is interesting to note

that Figure 6(a) clearly indicates the red-shift in the fundamental absorption edge with the increase of film thickness. The sharp absorption edge at wavelengths of approximately 370 nm is very close to the intrinsic band gap of ZnO (3.37 eV) and the red-shift of absorption edge will be also discussed in the later part.

No obvious interference fluctuations in the transmission spectra were observed in the ZnO nanorod thin films fabricated at 75 °C/4.5 and 6 h (one-step route), and 95 °C/1.5-6 h (multiple-stepwise route), as shown in Figs. 6(b) and 6(c). Based on the SEM photographs [Figs. 2(e)-(j)], these films are composed of a bundle of the ZnO nanorods with smaller diameter, and these ZnO nanorods do not coalesce together very well, which results in the formation of lots of unfilled inter-columnar volume and coarse surface in these ZnO nanorod thin films. In addition, some ZnO nanorods do not vertically align very well and they are inclined to the substrate surface. Therefore, the low transmittance and no fluctuation could be attributed to the incident light experiencing multiple random scattering between unfilled inter-columnar voids, inclined ZnO nanorods, and perpendicular ZnO nanorods in the poor-quality ZnO nanorod films. This effect leads to the destruction of the interference of multiple reflections, no obvious interference fluctuations in the transmission spectra and lower transmittance.

3.4.2 Refractive index and packing density

The refractive index (n) of the ZnO nanorod thin films were derived from the transmittance spectra using Swanepoel's method (Swanepoel, 1983). For those ZnO nanorod thin films with no obvious interference fluctuations in the transmission spectrum, the refractive index of can not be derived by Swanepoel's method. Figure 7 shows that the refractive index of ZnO nanorod thin films fabricated at 75 °C are strongly dependent on the growth time.

The refractive indices (n at λ = 550 nm) of the ZnO nanorod thin films fabricated at 75 °C for 3, 4.5, and 6 h are 1.70, 1.71, and 1.74, respectively. The increase in n of the ZnO nanorod thin films with rising growth time is considered as a result of the increase in compactness and crystallinity, which is consistent with previous XRD and SEM investigations.

In order to evaluate the extent of porosity presenting in the ZnO nanorod thin films, the packing density (P) was evaluated using the following Bragg–Pippard formula which is more suitable for the film with columnar or cylindrical grains (Harris et al., 1979).

$$n_f^2 = \frac{(1 - P)n_v^4 + (1 + P)n_v^2 n_b^2}{(1 + P)n_v^2 + (1 - P)n_b^2} \tag{4}$$

where P is expressed as the packing density. The n_f, n_v and n_b are the refractive indices of the porous films, the voids (n_v=1or empty voids) and the bulk materials, respectively.

After calculation, Figure 8 shows the variation of packing densities with growth time for the ZnO nanorod thin films grown at 75 °C. The packing densities of the ZnO nanorod thin films fabricated at 75 °C for 3 and 6 h increase from 0.81 to 0.84. The packing density increases with the increase of thickness and refractive index, and reaches to a maximum value at a film thickness of ~800 nm, which could be attributed to the significant reduction in the porosity and increase in the crystallinity [supporting SEM photographs, Figs. 2(a)-(d), and XRD pattern, Figure 4].

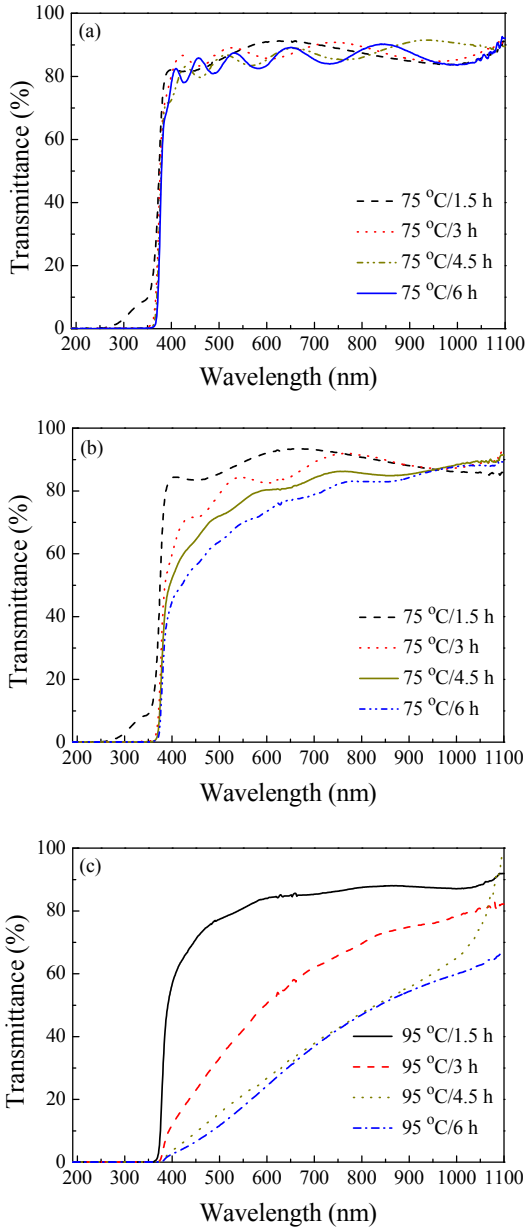

Fig. 6. Optical transmittance spectra of ZnO nanorod thin films fabricated under the conditions of 0.05 M, seed-layer grain size of ~20 nm, and (a) 75 °C/1.5-6 h (multiple-stepwise route), (b) 75 °C/1.5-6 h (one-step route), and (c) 95 °C/1.5-6 h (multiple-stepwise route).

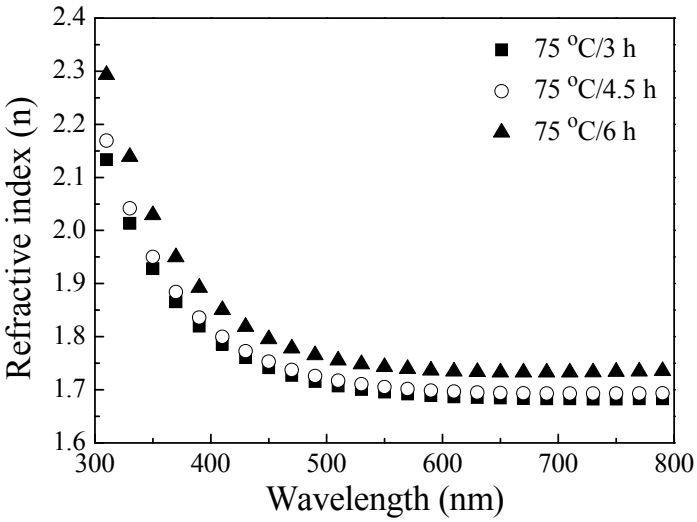

Fig. 7. Wavelength dependence of refractive index for ZnO nanorod thin films fabricated under the conditions of 0.05 M, seed-layer grain size of ~20 nm, multiple-stepwise route, and 75 °C/different growth time.

Because of the demands of compactness and high transmittance, most of the commercialized optical thin films are made by reactive sputtering technology under the high-vacuum and high-temperature condition. For comparisons, refractive indexes and packing densities of the sputtered ZnO films are quoted from some published reports. According to an investigation by Moustaghfir *et al.*, the refractive index (n at λ = 633 nm) and packing density of the radio frequency (r.f.) magnetron reactive sputtered ZnO film (a thickness of ~800 nm) fabricated under the sputtering conditions of a working pressure of 1 Pa, a r.f. power density of 0.89 Wcm^{-2}, Ar-O_2 ratio 95: 5, and the substrate temperature of room temperature (RT) were 1.89 and 0.93, respectively, and they could be enhanced to 1.91 and 0.94 by further annealing at 400 °C/1 h (Moustaghfir et al., 2003). Additionally, an earlier study of the r.f. magnetron reactive sputtered ZnO film (a thickness of 1000 nm) fabricated under the sputtering conditions of a working pressure of 1.33×10^{-2} m bar, a r.f. power of 500 W, Ar-O_2 ratio 40: 60, and the substrate temperature of room temperature (RT) by Mehan *et al.* revealed that the refractive indexes (n at λ = 550 nm) were 1.980 (n_{eb}: extra ordinary refractive index) and 1.963 (n_{ob}: ordinary refractive index), as well as packing densities were 0.986 and 0.978 (extra ordinary refractive index of bulk ZnO, n_{eb} = 2.006, and ordinary refractive index of bulk ZnO, n_{ob} = 1.990), respectively (Mehan et al., 2004). Although lots of parameters can influence the quality of sputtered ZnO films, such high refractive index and packing density may be the extreme values for the sputterred ZnO films. In our system, the optical transmittance (85 %), refractive index (1.74) and packing density (0.84) of optimum solution-growth ZnO nanorod thin film (a thickness of ~800 nm) is lower than that of the high-quality sputtered ZnO films. However, the solution-growth method is still a good technology for the fabrication of low-cost and low-temperature grown ZnO thin films.

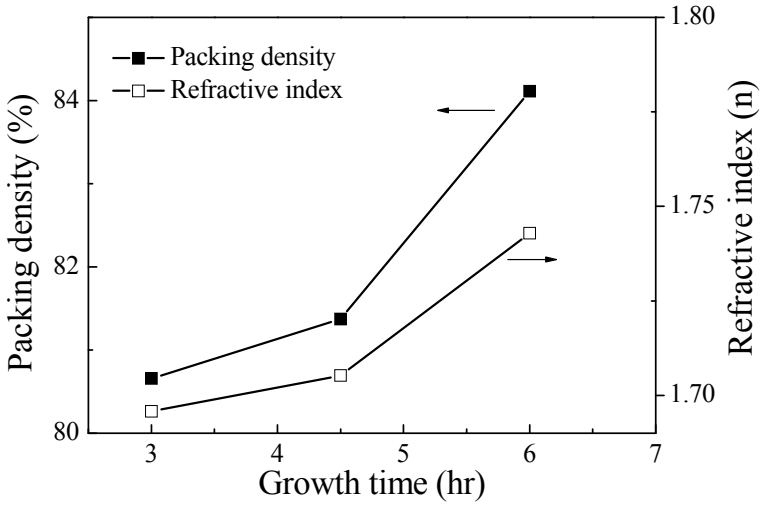

Fig. 8. Variation of packing densities and refractive indexes as a function of growth time for the ZnO nanorod thin films prepared under the conditions of 0.05 M, seed-layer grain size of ~20 nm, multiple-stepwise route, and 75 °C.

3.4.3 Photoluminescence spectra

Figure 9 shows the room temperature photoluminescence (PL) spectra of ZnO nanorod films fabricated at 75 °C/4.5 h, 75 °C/6 h, 95 °C/1.5 h, and 95 °C/3 h by multiple-stepwise route. The intense UV emission at 377-383 nm is due to the recombination of free excitons (Chen et al., 1998; Cho et al., 1999; Park et al., 2003). Obviously, the ZnO nanorod films prepared at 95 °C has more intense UV emission than that of ZnO nanorod films prepared at 75 °C. The intensity of UV emission is ascribed to film crystallinity, and the higher crystallinity possesses the higher intensity of UV emission (Wang & Gao, 2003). Compared the UV intensity of ZnO nanorod films prepared at 75 °C/6 h with that of the ZnO nanorod films prepared at 95 °C/1.5 h, these two films have similar thickness (~800 nm) and XRD diffraction intensities but the UV intensities are quite different. Therefore, the crystallinity of well-shaped hexagonal ZnO nanorod films prepared at 95 °C/1.5 h should be higher than that of ZnO nanorod films prepared at 75 °C/6 h even though the XRD diffraction intensities could not be used to make a judgment of crystallinity for these two films.

On the other hand, all of the PL spectra of ZnO nanorod films exhibit the obvious green-yellow emission at ~572 and ~600 nm, which are associated with the oxygen vacancies and oxygen interstitials, respectively (Ohashi et al., 2002; Studenikin et al., 1998; Wu et al., 2001). However, the ZnO nanorod films prepared at 75 °C had more intense green-yellow emission than that of ZnO nanorod films prepared at 95 °C, which indicates that the lower growth temperature could induce the formation of more oxygen vacancies and interstitials during the ZnO nanorods coarsen and aggregate together. In addition, the yellow emission of ZnO nanorod films prepared at 75 °C gradually dominated by increasing growth time, which indicates that the green emission and yellow emission compete with each other, and more oxygen interstitials are produced with increasing growth time and film thickness. The

above-mentioned PL phenomena imply that our most compact and highly c-axis-oriented ZnO nanorod films still possess lots of oxygen vacancies and interstitials.

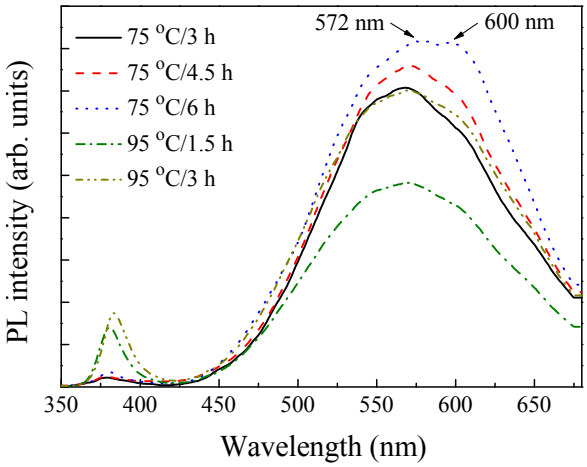

Fig. 9. Room temperature PL spectra of ZnO nanorod thin films fabricated under the conditions of 0.05 M, seed-layer grain size of ~20 nm, multiple-stepwise route, and different growth temperatures/time.

3.4.4 Optical band gap

The optical band gap (E_g) of the ZnO nanorod thin film which is a direct-transition-type semiconductor can be related to absorption coefficient (a) by

$$ahv = \text{const} \cdot (hv - E_g)^{1/2} \tag{5}$$

Here we assume the absorption coefficient $a=(1/d)\ln(1/T)$, where T is the transmittance and d is the film thickness (Serpone et al., 1995; Tan et al., 2005). Figure 10 plots the relationship of $(ahv)^2$ versus photon energy (E) of the ZnO nanorod thin films fabricated under 75 °C/3-6 h and the extrapolated optical band gaps of the films are determined. When the growth time increases from 3 to 6 h, the values o f E_g decrease from 3.35 to 3.31 eV which gradually diverges from the intrinsic band gap of ZnO (3.37 eV). It is known that the energy band gap of a ZnO thin film could be affected by the residual strain (Mohamed et al., 2006; Puchert et al., 1996; Srikant & Clarke, 1997), defects (Burstein, 1954; Dong et al., 2007; Moss, 1954; Sakai et al., 2006), and grain size confinement (Prathap et al., 2008; Wang et al., 2003). For ZnO nanorod thin films fabricated at 75 °C for 3 to 6 h, the average grain sizes enlarge from ~105 to ~200 nm and the film thicknesses increase from ~460 to ~800 nm, which results in the variation of strain from -0.26 to -0.32%. In addition, the PL intensity of yellow emission gradually increases and the more oxygen interstitials are produced. Prathap *et al*. found the energy band gaps increased with the increase of film thickness and grain size in ZnS films fabricated by thermal evaporation (Prathap et al., 2008). Wang *et al*. also observed that the peak position of free excitonic emission redshifted from 3.3 to 3.2 eV with an increase of grain size from 21 to 64 nm, which could be attributed to the quantum confinement effect

(Wang et al., 2003). Although many factors influence the variation of energy band gap, in our system the energy band gaps increasing with the increase of film thickness might be related to the dependence of enhanced strain, enlarged grain size and more oxygen interstitials.

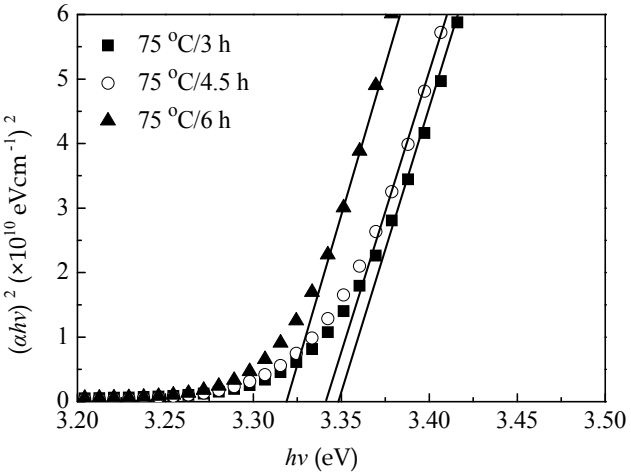

Fig. 10. $(\alpha h\nu)^2$ as a function of photon energy for the ZnO nanorod thin films prepared under the conditions of 0.05 M, seed-layer grain size of ~20 nm, multiple-stepwise route, 75 °C, and different growth time.

4. Conclusion

Highly c-axis-oriented ZnO nanorods thin films were obtained on silica glass substrates by a simple solution-growth technique. The fabrication of highly dense ZnO nanorod thin films are highly dependent on the different zinc ion concentrations, growth temperatures, growth time, growth routes, and ZnO seed-layer morphologies. The higher zinc ion concentrations, growth temperature, and growth time can induce ZnO nanorods with larger diameter and length. The most compact and vertically-aligned ZnO nanorod thin film with the thickness of ~800 nm and average hexagonal grain size of ~200 nm exhibits the extremely C-axis orientation, average visible transmittance 85%, refractive index 1.74, packing density 0.84, and energy band gap 3.31 eV, and it was fabricated under the optimum parameters: 0.05 M, 75 °C, 6 h, multiple-stepwise, and ZnO seed layer with an average grain size of ~20 nm. The photoluminescence spectrum indicates that the densest ZnO nanorod thin film possesses lots of oxygen vacancies and interstitials.

As we demonstrate here, the solution-growth technique is a non-vacuum, low-temperature, low-cost, large-scale, easily controlled process for the fabrication of high-quality, optical-grade ZnO thin films with highly compact ZnO nanorod arrays. In particular, this process can operate at low temperature without organic binders/surfactants or further heat treatment, and thus can be applied to flexible electronics.

5. Acknowledgement

The author would like to thank the National Science Council of the Republic of China for financially supporting this research under Contract No. NSC 96-2221-E-194-042-MY2.

6. References

Burstein, E. (1954). Anomalous Optical Absorption Limit in InSb. *Phys. Rev.,* Vol. 93, No. 3, (Feb 1954), pp. (632-633), ISSN 0031-899X.

Chen, Y., Bagnall, D.M., Koh, H.J., Park, K.T., Hiraga, K., Zhu, Z., & Yao, T. (1998). Plasma Assisted Molecular Beam Epitaxy of ZnO on C-Plane Sapphire: Growth and Characterization. *J. Appl. Phys.,* Vol. 84, No. 7, (Oct 1998), pp. (3912-3918), ISSN 0021-8979.

Cho, S., Ma, J., Kim, Y., Sun, Y., Wong, G.K.L., Ketterson, J.B. (1999). Photoluminescence a and Ultraviolet Lasing of Polycrystalline ZnO Thin Films Prepared by the Oxidation of the Metallic Zn. *Appl. Phys. Lett.*, Vol. 75, No. 18, (Nov 1999), pp. (2761-2763), ISSN 0003-6951.

Dong, B.Z., Fang, G.J., Wang, J.F., Guan, W.J., & Zhao, X.Z. (2007). Effect of Thickness on Structural, Electrical, and Optical Properties of ZnO: Al Films Deposited by Pulsed Laser Deposition. *J. Appl. Phys.,* Vol. 101, No. 3, (Feb 2007), pp. (033713-1-033713-7), ISSN 0021-8979.

Harris, M., Macleod, H.A., Ogura, S., Pelletier, E., & Vidal, B. (1979). In-Situ Ellipsometric Monitor with Layer-by-Layer Analysis for Precise Thickness Control of EUV Multilayer Optics. *Thin Solid Films,* Vol. 57, No. 1, (Feb 1979), pp. (173-178), ISSN 0040-6090.

Henley, S.J., Ashfold, M.N.R., & Cherns, D. (2004). The Growth of Transparent Conducting ZnO Films by Pulsed Laser Ablation. *Surf. Coat. Technol.,* Vol. 177-178, (Jan 2004), pp. (271-276), ISSN 0257-8972.

Jeong, S.H., Kim, B.S., & Lee, B.T. (2003). Photoluminescence Dependence of ZnO Films Grown on Si(100) by Radio-Frequency Magnetron Sputtering on the Growth Ambient. *Appl. Phys. Lett.,* Vol. 82, No. 16, (Apr 2003), pp. (2625-2627), ISSN 0003-6951.

Kishimoto, H., Takahama, K., Hashimoto, N., Aoib, Y. & Deki, S. (1998). Photocatalytic Activity of Titanium Oxide Prepared by Liquid Phase Deposition (LPD). *J. Mater. Chem.,* Vol. 8, No. 9, (Feb 1998), pp. (2019-2024), ISSN 0959-9428.

Kligshirn, C. (1975). The Luminescence of ZnO under High One-and Two-Quantum Excitation. *Phys. Status Solidi B,* Vol. 71, No. 2, (Oct 1975), pp. (547-556), ISSN 0370-1972.

Lee, J.C., Kang, K.H., Kim, S.K., Yoon, K.H., Song, J.S., & Park, I.J. (2000). RF Sputter Deposition of the High-Guality Intrinsic and N-Type ZnO Window Layers for Cu(In,Ga)Se2-Based Solar Cell Applications. *Sol. Energy Mater. Sol. Cells,* Vol. 64, No. 2, (Sep 2000), pp. (185-195), ISSN 0927-0248.

Lee, Y.J., Sounart, T.L., Scrymgeour, D.A., Voigt, J.A., & Hsu, J.W.P. (2007). Control of ZnO Nanorod Array Alignment Synthesized Via Seeded Solution Growth. *J. Cryst. Growth.,* Vol. 304, No. 1, (Jun 2007), pp. (80-85), ISSN 0022-0248.

Li, Q., Kumar, V., Li, Y., Zhang, H., Marks, T.J., & Chang, R.P.H. (2005). Fabrication of ZnO Nanorods and Nanotubes in Aqueous Solutions. *Chem. Mater.,* Vol. 17, No. 5, (Mar 2005), pp. (1001-1006), ISSN 0897-4756.

Lin, J.M., Hsu, M.C., & Fung, K. Z. (2006). Deposition of ZrO2 Film by Liquid Phase Deposition. *J. Power Sources,* Vol. 159, No. 1, (Sep 2006), pp. (49-54), ISSN 0378-7753.

Mehan, N., Gupta, V., Sreenivas, K., & Mansinght, A. (2004). Effect of Annealing on Refractive Indices of Radio-Frequency Magnetron Sputtered Waveguiding Zinc Oxide Films on Glass. *J. Appl. Phys.,* Vol. 96, No. 6, (Sep 2004), pp. (3134-3139), ISSN 0021-8979.

Mirica, E., Kowach, G., Evans, P., & Dut, H. (2004). Morphological Evolution of ZnO Thin Films Deposited by Reactive Sputtering. *Cryst. Growth. Des.,* Vol. 4, No. 1, (Sep 2004) pp. (147-156), ISSN 1528-7483

Mohamed, S.H., El-Rahman, A.M.A., & Salem, A.M. (2006). Effect of rf Plasma Nitriding Time on Electrical and Optical Properties of ZnO Thin Films. *J. Phys. Chem. Solids.,* Vol. 67, No. 11, (Nov 2006) pp. (2351-2357), ISSN 0022-3697.

Moss, T.S. (1954). The Interpretation of the Properties of Indium Antimonide. *Proc. Phys. Soc. B,* Vol. 67, No. 10, (Oct 1954), pp. (775-782), ISSN 0370-1328

Moustaghfir, A., Tomasella, E., Amor, S.B., Jacquet, M., Cellier, J., & Sauvaget, T. (2003). Structural and Optical Studies of ZnO Thin Films Deposited by r.f. Magnetron Sputtering: Influence of Annealing. *Surf. Coat. Technol.*, Vol. 174-175, (Oct 2003), PP. (193-194), ISSN 0257-8972.

Mugdur, P.H., Chang, Y.-J., Han, S-.Y., Su, Y-W., Morrone, A.A., Ryu, S.O., Lee, T.-J., & Chang, C.-H. (2007). A Comparison of Chemical Bath Deposition of CdS from a Batch Reactor and a Continuous-Flow Microreactor. *J. The Electrochem. Soc.*, Vol. 154, No. 9, (Jul 2007), pp. (D482-D488), ISSN 0013-4651.

Özgür, Ü., Alivov, Y.I., Liu, C., Teke, A., Reshchikov, M.A., Doğan, S., Avrutin,V., Cho, S.-J., & Morkoç, H. J. (2005). A Comprehensive Review of ZnO Materials and Devices. *J. Appl. Phys.,* Vol. 98, No. 4, (Aug 2005), PP. (041301-1-041301-103), ISSN 0021-8979.

Puchert, M.K., Timbrell, P.Y., & Lamb, R.N. (1996). Postdeposition Annealing of Radio Frequency Magnetron Sputtered ZnO Films. *J. Vac. Sci. Technol. A*, Vol. 14, No. 4, (Aug 1996), PP. (2220-2230), ISSN 0734-2101.

Park, W.I., Jun, Y.H., Jung, S.W., & Yia, G.C. (2003). Excitonic Emissions Observed in ZnO Single Crystal Nanorods. *Appl. Phys. Lett.*, Vol. 82, No. 6, (Feb 2003), pp. (964-966), ISSN 0003-6951.

Prathap, P., Revathi1, N., Subbaiah, Y.P.V., & Reddy, K.T.R. (2008). Thickness Effect on the Microstructure, Morphology and Optoelectronic Properties of ZnS Films. *J. Phys.: Condens. Matter*, Vol. 20, No. 3, (Dec 2008), pp. (035205-1-035205-10), ISSN 0953-8984

Puchert, M.K., Timbrell, P.Y., & Lamb, R.N. (1996). Postdeposition Annealing of Radio Frequency Magnetron Sputtered ZnO Films. *J. Vac. Sci. Technol. A*, Vol. 14, No. 4, (Aug 1996), pp. (2220-2230), ISSN 0734-2101.

Sagar, P., Shishodia, P.K., Mehra, R.M., Okada, H., Wakahara, A., & Yoshidat, A. (2007). Photoluminescence and Absorption in Sol–Gel-Derived ZnO Films. *J. Lumin.*, Vol. 126, No. 2, (Oct 2007), pp. (800-806). ISSN 0022-2313.

Saito, N., Haneda, H., Sekiguchi, T., Ohashi, N., Sakaguchi, I., & Koumoto, K. (2002). Low-Temperature Fabrication of Light-Emitting Zinc Oxide Micropatterns Using Self-

Assembled Monolayers. *Adv. Mater.*, Vol. 14, No. 6, (Mar 2002), pp. (418-421), ISSN 935-9648.

Sakai, K., Kakeno, T., Ikari, T., Shirakata, S., Sakemi, T., Awai, K., & Yamamoto, T. (2006). Defect Centers and Optical Absorption Edge of Degenerated Semiconductor ZnO Thin Film Grown by a Reactive Plasma Deposition by Means of Piezoelectric Photothermal Spectroscopy. *J. Appl. Phys.*, Vol. 99, No. 4, (Feb 2006), pp. (043508-1-043508-7), ISSN 0021-8979.

Ohgaki, N., Sekiguchi, T., Aoyama, K., Ohgaki, T., Terada, Y., Sakaguchi, I., Tsurumi, T., & Haneda, H. J. (2001). Band-Edge Emission of Undoped and Doped ZnO Single Crystals at Room Temperature. *J. Appl. Phys.*, Vol. 91, No. 6, (Mar 2002), pp.(3658-3663), ISSN 0021-8979.

Serpone, N., Lawless, D., & Khairutdinov, Rr. (1995). Size Effects on the Photophysical Properties of Colloidal Anatase Ti02 Particles: Size Quantization or Direct Transitions in This Indirect Semiconductor?. *J. Phys. Chem.*, Vol. 99, No. 45, (Nov 1995), pp. (16646-16654). ISSN 0022-3654.

Srikant, V., Clarke, D.R. (1997). Optical Absorption Edge of ZnO Thin Films: The Effect of Substrate. *J. Appl. Phys.*, Vol. 81, No. 6357, (May 1997), pp. (6357-6364), ISSN 0021-8979.

Studenikin, S.A., Golego, N., & Cocivera, M. (1998). Fabrication of Green and Orange Photoluminescent, Undoped ZnO Films Using Spray Pyrolysis. *J. Appl. Phys.*, Vol. 84, No. 4, (Aug 1998), pp. (2287-2294), ISSN 0021-8979.

Swanepoel,R. (1983). Determination of the Thickness and Optical Constants of Amorphous Silicon. *J. Phys. E: Sci. Instrum.,* Vol. 16, No. 12, (Dec 1983), pp.(1214-1222), ISSN 0022-3735.

Tak, Y., Yong, K.J. (2005). Controlled Growth of Well-Aligned ZnO Nanorod Array Using a Novel Solution Method. *J. Phys. Chem. B*, Vol. 109, No. 41, (Oct 2005), pp. (19263-19269), ISSN 1089-5647.

Tan, S.T., Chen, B.J., Sun, X.W., Fan, W.J., Kwok, H.S., Zhang, X.H., & Chua, S.J. (2005). Blueshift of Optical Band Gap in ZnO Thin Films Grown by Metal-Organic Chemical-Vapor Deposition. *J. Appl. Phys.*, Vol. 98, No. 013505, (Jul 2005), pp. (013505-1-013505-5), ISSN 0021-8979.

Tsukuma, K., Akiyama, T., & Imai, H. (1997). Liquid Phase Deposition Film of Tin Oxide. *J. Non-Cryst Solids,* Vol. 210, No. 1, (Feb 1997), pp. (48-54), ISSN 0022-3093.

Vayssieres, L., Keis, K., Lindquist, S. E., & Hagfeldt, A. J. (2001). Purpose-Built Anisotropic Metal Oxide Material: 3D Highly Oriented Microrod Array of ZnO. *J. Phys. Chem. B*, Vol. 105 , No. 17, (May 2001), pp. (3350-3352), ISSN 1089-5647.

Vayssieres, L. (2003). Growth of Arrayed Nanorods and Nanowires of ZnO from Aqueous Solution**. *Adv. Mater.*, Vol. 15, No. 5, (Mar 2003), pp. (464-466), ISSN 1521-4095.

Wang, J. M., Gao, L. J. (2003). Wet Chemical Synthesis of Ultralong and Straight Single-Crystalline ZnO Nanowires and Their Excellent UV Emission Properties. *J. Mater. Chem.*, Vol. 13, No. 10, (Aug 2003), pp. (2551-2254), ISSN 0959-9428.

Wang, Y.G., Lau, S.P., Lee, H.W., Yu, S.F., Tay, B.K., Zhang, X.H., & Hng, H.H. (2003). Photoluminescence Study of ZnO Films Prepared by Thermal Oxidation of Zn Metallic Films in Air. *J. Appl. Phys.*, Vol. 94, No. 1, (Jul 2003), pp. (354-358), ISSN 0021-8979.

Wu, X.L., Siu, G.G., Fu, C.L., & Ong, H.C. (2001). Photoluminescence and Cathodoluminescence Studies of Stoichiometric and Oxygen-Deficient ZnO Films. *Appl. Phys. Lett.*, Vol. 78, No. 16, (Apr 2001), pp. (2285-2287), ISSN 0003-6951.

Yang, J.L., An, S.J., Park, W.I., Yi, G.C., & Choi, W. (2004). Photocatalysis Using ZnO Thin Films and Nanoneedles Grown by Metal-Organic Chemical Vapor Deposition**. *Adv. Mater.*, Vol. 16, No. 18, (Sep 2004), pp. (1661-1664), ISSN 1521-4095.

Zhao, J., Jin, Z.G., Li, T., & Liu, X.X. (2006). Nucleation and Growth of ZnO Nanorods on the ZnO-Coated Seed Surface by Solution Chemical Method. *J. Eur. Ceram. Soc.*, Vol. 26, No. 13, (Sep 2005), pp. (2769-2775), ISSN 0955-2219.

Zhu, Y.W., Zhang, H.Z., Sun, X.C., Feng, S.Q., Xu, J., Zhao, Q., Xiang, B., Wang, R.M., & Yua, D.P. (2003). Efficient Field Emission from ZnO Nanoneedle Arrays. *Appl. Phys. Lett.*, Vol. 83, No. 1, (Jul 2003), pp. (144-146), ISSN 0003-6951.

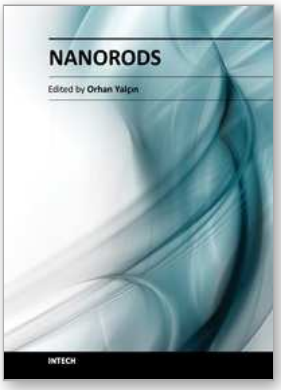

Nanorods

Edited by Dr. Orhan Yalçın

ISBN 978-953-51-0209-0
Hard cover, 250 pages
Publisher InTech
Published online 09, March, 2012
Published in print edition March, 2012

The book "Nanorods" is an overview of the fundamentals and applications of nanosciences and nanotechnologies. The methods described in this book are very powerful and have practical applications in the subjects of nanorods. The potential applications of nanorods are very attractive for bio-sensor, magneto-electronic, plasmonic state, nano-transistor, data storage media, etc. This book is of interest to both fundamental research such as the one conducted in Physics, Chemistry, Biology, Material Science, Medicine etc., and also to practicing scientists, students, researchers in applied material sciences and engineers.

INTECH
open science | open minds

InTech Europe
University Campus STeP Ri
Slavka Krautzeka 83/A
51000 Rijeka, Croatia
Phone: +385 (51) 770 447
Fax: +385 (51) 686 166
www.intechopen.com

InTech China
Unit 405, Office Block, Hotel Equatorial Shanghai
No.65, Yan An Road (West), Shanghai, 200040, China
中国上海市延安西路65号上海国际贵都大饭店办公楼405单元
Phone: +86-21-62489820
Fax: +86-21-62489821